Earth's Variable Rotation

RAYMOND HIDE AND JEAN O. DICKEY*

Recent improvements in geodetic data and practical meteorology have advanced research on fluctuations in the Earth's rotation. The interpretation of these fluctuations is inextricably linked with studies of the dynamics of the Earth-moon system and dynamical processes in the liquid metallic core of the Earth (where the geomagnetic field originates), other parts of the Earth's interior, and the hydrosphere and atmosphere. Fluctuations in the length of the day occurring on decadal time scales have implications for the topography of the core-mantle boundary and the electrical, magnetic, and other properties of the core and lower mantle. Investigations of more rapid fluctuations bear on meteorological studies of interannual, seasonal, and intraseasonal variations in the general circulation of the atmosphere and the response of the oceans to such variations.

FUTURE ADVANCES IN RESEARCH ON THE INTERPRETATION of Earth rotation fluctuations will be inseparable from progress toward a better understanding of the structure and dynamics of all parts of the Earth. Herein lies the fascination of this highly interdisciplinary area of Earth sciences. As Earth rotation and other geophysical observations continue to improve in accuracy, frequency, and coverage, so will our ability to exploit new data in both geophysical research and applications to problems of forecasting the behavior of our planet. Central to these activities will be extensions of current programs of Earth rotation observations, with emphasis in the immediate future on the study of rapid changes and exploiting the most recent improvements in observational techniques.

Define $\mathbf{\Omega}$ as the angular velocity with which a geographical reference frame based on observatories fixed to the Earth's crust rotates relative to an inertial frame based on the fixed stars. Precise determinations of $\mathbf{\Omega}$ by geodesists and astronomers reveal temporal fluctuations over time scales ranging from days to centuries and longer; the interpretation of these fluctuations in terms of basic dynamical processes has for many years engaged the attention of workers in astronomy and in several areas of Earth sciences, including meteorology, oceanography, and geophysics.

Modern methods for determining $\mathbf{\Omega}(t)$ (where t denotes time based on atomic clocks) exploit the techniques of very long baseline interferometry (VLBI), involving positional observations of distant quasars at radio wavelengths, and satellite laser ranging (SLR) and lunar laser ranging (LLR), involving, respectively, laser ranging to artificial satellites and corner reflectors placed on the moon by the astronauts. By providing details of the time series of all three components of $\mathbf{\Omega}(t)$ that were unobtainable from earlier optical observations, the new methods are sharpening old questions and raising new ones. Research on the Earth's rotation is facilitated by the collection and dissemination of $\mathbf{\Omega}(t)$ observations by the International Earth Rotation Service in Paris, working under the auspices of the International Astronomical Union and the International Union of Geodesy and Geophysics.

Theoretical studies of fluctuations in $\mathbf{\Omega}(t)$ are based on the application of Euler's dynamical equations to the problem of finding the response of a slightly deformable solid Earth to a variety of surface and internal stresses. The details can be quite complicated, but general physical considerations suffice to show that the fluctuations must be manifestations of (i) changes in the moment of inertia of the solid Earth due to redistribution of matter within it and (ii) the action of net torques resulting from applied stresses (*1–13*). Contributions to the former comprise (i) periodic tidal deformations of the solid Earth produced by the gravitational action of the moon, sun, and other astronomical bodies, (ii) nonperiodic deformations due to surface stresses produced by fluctuating fluid flow in the underlying liquid metallic core and the overlying hydrosphere and atmosphere, and (iii) nonperiodic mass redistribution associated with earthquakes, the melting of ice, and, on geological time scales, mantle convection and movements of tectonic plates.

One important contribution to the applied torques acting on the solid Earth arises from the gravitational action of the sun and moon on the Earth's tidal bulge, which, owing to tidal friction within the oceans and other parts of the Earth, is oriented at an angle to the line joining the centers of the interacting bodies. The Earth's rotation speed is thus decelerated at a rate corresponding to a gradual lengthening of the day,

$$\Lambda(t) \equiv 2\pi/|\mathbf{\Omega}(t)| \qquad (1)$$

by about 1.4 ms per century. As a result, the moon's orbit expands at a detectable rate of 3.7 ± 0.2 cm per year. Stronger torques (by a factor of about 50), which fluctuate irregularly in magnitude and sign on time scales of several years and upwards, are thought to be produced by core motions.

It has been argued on general quantitative grounds that such motions provide the most likely source for the excitation of irregular fluctuations in $\mathbf{\Omega}(t)$ on decadal time scales. Decadal changes in the length of the day (LOD) range in amplitude to 5 ms; concomitant displacements of the pole of the rotation axis of the solid Earth relative to the geographical axis amount to a few meters. But by far the strongest torques to which the solid Earth is subjected are those generated by atmospheric motions. These torques act directly over continental regions through the fluctuating tangential viscous stress-

R. Hide is with the Robert Hooke Institute, The Observatory, Clarendon Laboratory, Parks Road, Oxford OX1 3PU, United Kingdom. J. O. Dickey is with the Jet Propulsion Laboratory, California Institute of Technology, Mail stop 238-332, Pasadena, CA 91109.

*To whom correspondence should be addressed.

es and normal pressure forces in the surface boundary layers and indirectly over the oceans. Concomitant changes in the angular momentum associated with the global atmospheric super-rotation at about 10 m s^{-1} relative to the underlying planet are accompanied by compensating changes in $\Lambda(t)$ of up to about 1 ms on interannual, seasonal, and intraseasonal time scales. Nonaxial torques associated with fluctuations in nonaxisymmetric features of global atmospheric pressure and wind fields excite movements of the pole at amplitudes up to several meters, including a significant part of the Chandlerian polar motion at the solid Earth's free wobble period of 14 months (*1–15*).

Consider a frame of reference fixed in the solid Earth with its origin at the Earth's center of mass and aligned with the principal axes of the solid Earth (Fig. 1). The body-fixed frame rotates with instantaneous angular velocity $\omega_i(t)$, where

$$\omega_i(t) \equiv \mathbf{\Omega}(t) \equiv \Omega_0[m_1(t), m_2(t), 1 + m_3(t)] \quad (2)$$

and $\Omega_0 \equiv 2\pi/\Lambda_0$ and $\Lambda_0 \equiv 86{,}400$ s. This equation for $\omega_i(t)$ defines the geodetic quantities m_i, $i = 1, 2, 3$. The movement of the Earth's pole of rotation relative to the (geographical) body-fixed axes is given by $m_1(t)$ and $m_2(t)$; variations in the LOD are related to m_3 through the expression $\Lambda(t) \equiv \Lambda_0/[1 + m_3(t)]$ (Fig. 1).

Our ability to separate the $\mathbf{\Omega}(t)$ time series into components of meteorological and nonmeteorological origin has been revolutionized by the availability of routine determinations of all three components of the angular momentum of the atmosphere, $H^A{}_i(t)$, $i = 1, 2, 3$ (Fig. 1). The quantities $\chi_i(t)$, $i = 1, 2, 3$ (Fig. 1), are dimensionless measures of $H^A{}_i(t)$ introduced in (*16*) to facilitate the assessment of meteorologically induced changes in $\omega_i(t)$. Daily or twice daily determinations of $\chi_i(t)$ are now produced from the output of weather prediction models from various meteorological centers in the United States, United Kingdom, and Japan. Determinations of the equatorial components χ_1 and χ_2 (Fig. 1) have stimulated much research on the excitation of the Earth's polar motion (*5, 14–17*), but the discussion of these new developments lies beyond the scope of this article. We summarize below recent progress on the determination from geodetic data of the various spectral components into which the LOD time series $\Lambda(t)$ can conveniently be separated, and we then consider the interpretation of these components in terms of the underlying geophysical processes responsible for their excitation.

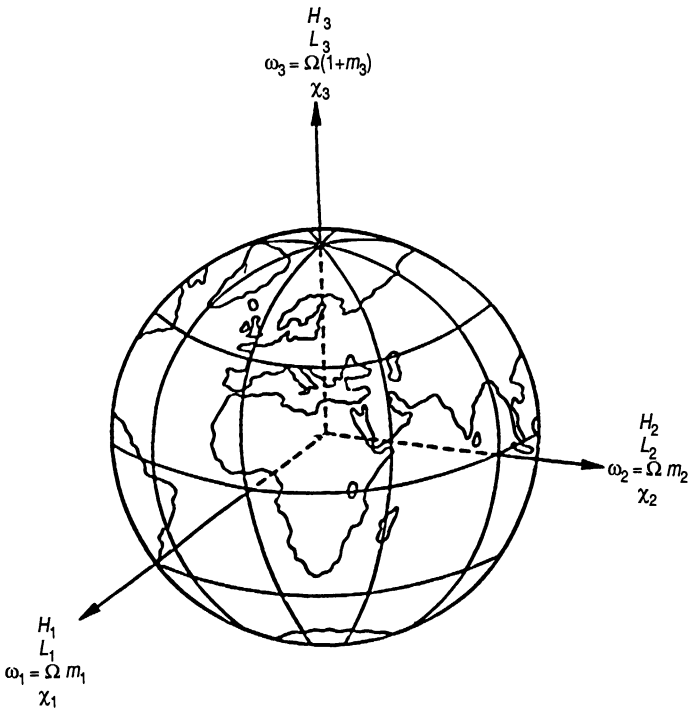

Fig. 1. The components of the vectors ω_i, H_i, and L_i and the dimensionless pseudovectors m_i, and χ_i. The symbol ω_i represents the angular velocity of the solid Earth relative to an inertial frame, H_i is the angular momentum of the atmosphere, and L_i is the net torque acting upon it [see (*97*), figure 1].

Spectrum of Irregular LOD Fluctuations

The quantity of interest in the study of irregular LOD fluctuations is

$$\Lambda^*(t) \equiv \Lambda(t) - \Lambda_0 - \Lambda_1(t) - \Lambda_2(t) \quad (3)$$

rather than the full $\Lambda(t)$ time series. Here $\Lambda_1(t)$ is the long-term increase in $\Lambda(t)$ at 1.4×10^{-3} s per century associated with tidal friction (see above) and $\Lambda_2(t)$ is a sum of strictly periodic terms with amplitudes of up to 0.5 ms at known tidal frequencies. Changes in the moment of inertia that are associated with $\Lambda_2(t)$ are attributable to calculable distortions in the figure of the Earth produced by the gravitational action of the moon and sun (*18*).

The residual time series $\Lambda^*(t)$, representing irregular fluctuations on time scales ranging from decades to days, is conveniently expressed as the sum of four terms:

$$\Lambda^*(t) \equiv \Lambda_\alpha(t) + \Lambda_\beta(t) + \Lambda_\gamma(t) + \Lambda_\delta(t) \quad (4)$$

denoting respectively the decadal, interannual, seasonal, and intraseasonal components (*19, 20*). They are largely attributable to processes that effect the exchange on various time scales of angular momentum between the solid Earth and the fluid regions with which it interacts at its upper and lower surfaces. The interactions are produced by normal and tangential hydrodynamical stresses acting at these interfaces (see below) that give rise to a net axial torque $\hat{\Gamma}^*(t)$. It is convenient to introduce the hypothetical equivalent axial torque

$$\Gamma^*(t) \equiv -2\pi C\dot{\Lambda}^*(t)/\Lambda_0{}^2 \quad (5)$$

where $\dot{\Lambda}^*(t) \equiv d\Lambda^*(t)/dt$ and $C = 7.04 \times 10^{37}$ kg m^2 is the principal moment of inertia of the solid Earth (mantle, crust, and cryosphere) about the polar axis, which amounts to 0.9 times that of the whole Earth (to which the solid inner core, liquid outer core, hydrosphere, and atmosphere contribute $7 \times 10^{-4}\, C$, $10^{-1}\, C$, $3 \times 10^{-4}\, C$, and $10^{-6}\, C$, respectively). The actual axial torque $\hat{\Gamma}^*(t)$ acting on the solid Earth would be exactly the same as $\Gamma^*(t)$ in the hypothetical case when it is possible to neglect effects due to (i) departures from perfect rigidity of the solid Earth and (ii) motions in other parts of the Earth induced by fluctuations in the rotation of the solid Earth. In practice, $\Gamma^*(t)$ differs from $\hat{\Gamma}^*(t)$ by no more than about 10%. Analogously to Eq. 4, $\Gamma^*(t)$ can be expressed as the sum of spectral components

$$\Gamma^*(t) = \Gamma_\alpha(t) + \Gamma_\beta(t) + \Gamma\gamma(t) + \Gamma_\delta(t) \quad (6)$$

where $\Gamma_\alpha(t) \equiv -2\pi C\, \dot{\Lambda}_\alpha(t)/\Lambda^2{}_0$, and so forth (see Eq. 4).

Determinations of $\Lambda^*(t)$ and $\Gamma^*(t)$ and their representations in terms of spectral components are presented in Figs. 2 to 5. In the modern period (Fig. 2), the data used were the Jet Propulsion Laboratory's (JPL's) Kalman-filtered series, which combines Earth rotation results from optical astrometry and the space geodetic techniques of VLBI and LLR to form a high-quality series in which the issues of reference frames and the unevenness of data quality and quantity have been adequately addressed (*21, 22*). Optical data dominate the early portion of the series; modern space geodetic measurements started in the 1970s (LLR in 1970 and VLBI in

1978). Owing to the improvement with time of the availability of high-frequency information, the error of the $\Lambda^*(t)$ time series decreases significantly with time.

Long-term data are needed to address many questions; however, the quality of data varies with time. In order to study LOD variations before 1962 (Fig. 3), lunar occultation observations were utilized for the period 1860 through 1956, whereas photozenith tube measurements were used for the period of 1957 through 1962. Before 1925, the uncertainty in the interannual variations was comparable in size to the variation itself (*19*), and as a consequence the estimated interannual torques before 1925 may not be reliable, for they are dominated by effects due to measurement noise.

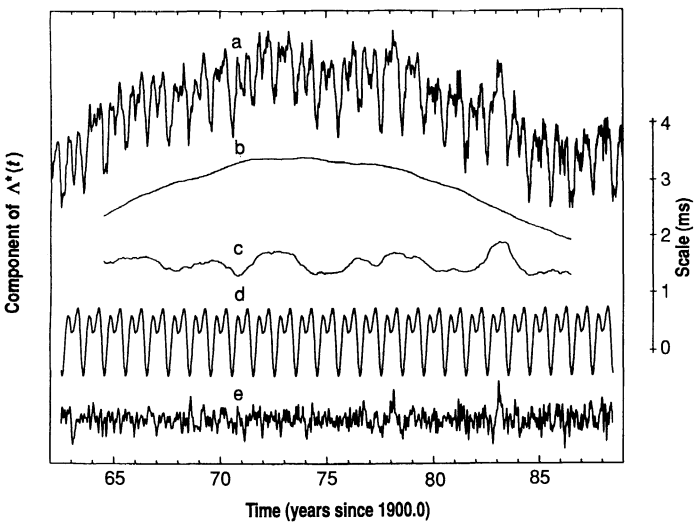

Fig. 2. Time series of irregular fluctuations $\Lambda^*(t)$ in the length of the day from 1963 to 1988 (curve a) and its decadal $[\Lambda_\alpha(t)]$ (see also Fig. 3), interannual $[\Lambda_\beta(t)]$, seasonal $[\Lambda_\gamma(t)]$, and intraseasonal $[\Lambda_\delta(t)]$ components (curves b, c, d, and e, respectively). The component $\Lambda_\alpha(t)$ largely reflects angular momentum exchange between the solid Earth and the underlying liquid metallic outer core (see also Fig. 3) produced by torques acting at the core-mantle boundary (see Figs. 4 and 5). The components $\Lambda_\beta(t)$, $\Lambda_\gamma(t)$, and $\Lambda_\delta(t)$ largely reflect angular momentum exchange between the atmosphere and the solid Earth produced by torques acting directly on the solid Earth over continental regions of the Earth's surface and indirectly over oceanic regions.

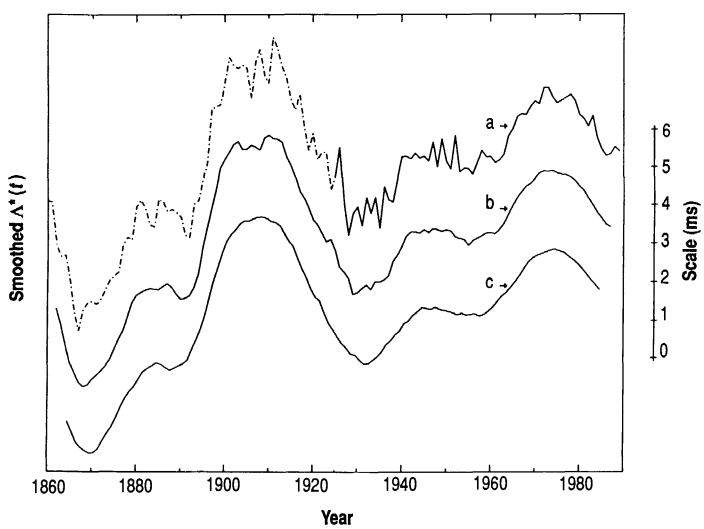

Fig. 3. Smoothed $\Lambda^*(t)$ time series using 1-year, 5-year, and 10-year running means (curves a, b, and c), computed from the $\Lambda^*(t)$ time series based on lunar occultation observations (*93*), smoothed as in (*94*) for the period 1860 to 1943, on a Kalman smoothing of monthly lunar occultation data for 1944 to 1956 (*95, 96*), photozenith tube measurements for 1957 through 1962 (*94*), and the JPL Kalman filter series after 1962 (Fig. 2). The LOD data for the entire period (1860 to 1989) are based on annual values centered at the beginning of each calendar year.

Variability of the LOD on all time scales, from days to decades, is evident in Figs. 2 and 3. The clear parabolic trend in $\Lambda_\alpha(t)$ from 1962 to 1988 (Fig. 2, curve b), taken to be the 5-year running mean of $\Lambda^*(t)$, is a part of the more complicated variations visible over longer periods (Fig. 3). We obtained the interannual component $\Lambda_\beta(t)$ (Fig. 2, curve c) by taking the difference between the 1-year and 5-year running mean values of the $\Lambda^*(t)$ time series, an efficient procedure for filtering out the seasonal cycle. The difference between $\Lambda^*(t)$ and the sum $\Lambda_\alpha(t) + \Lambda_\beta(t)$ constitutes the residual of Λ^* from its annual running mean and is further decomposed into the sum of the average seasonal component $\Lambda_\gamma(t)$, obtained by averaging the data with respect to the seasonal cycle over the time interval considered (Fig. 2, curve d) and the irregular intraseasonal component $\Lambda_\delta(t)$ (Fig. 2, curve e).

The seasonal and intraseasonal $[\Lambda_\gamma(t)$ and $\Lambda_\delta(t)]$ components of $\Lambda^*(t)$ are largely due to angular momentum exchange between the atmosphere and the solid Earth, and there is strong evidence that meteorological excitation is also the main cause of interannual fluctuations $[\Lambda_\beta(t)]$. However, the decadal variations $\Lambda_\alpha(t)$ are too large in amplitude to be attributable to angular momentum exchange between the atmosphere (or the hydrosphere or both) and the solid Earth, but a case can be made that they are excited by motions in the Earth's liquid core.

Decadal Fluctuations

Observations of the main geomagnetic field indicate that irregular magnetohydrodynamic flow occurs in the Earth's liquid metallic core with typical speeds of about 3×10^{-4} m s^{-1}; associated horizontal pressure variations on a planetary scale are about 3×10^2 N m^{-2}. It is accepted on general quantitative grounds that fluctuations in these motions give rise to angular momentum exchange between the liquid core and overlying "solid" mantle and that the observed decadal variation $\Lambda_\alpha(t)$ is largely a manifestation of that exchange (*1–4, 10, 12, 13, 23–31*). But in contrast with studies of meteorological excitation of the more rapid components $\Lambda_\beta(t)$, $\Lambda_\gamma(t)$, and $\Lambda_\delta(t)$ of the $\Lambda^*(t)$ spectrum, knowledge of core motions is insufficiently detailed for one to make determinations of the net torque acting at the core-mantle boundary (CMB) by calculating the

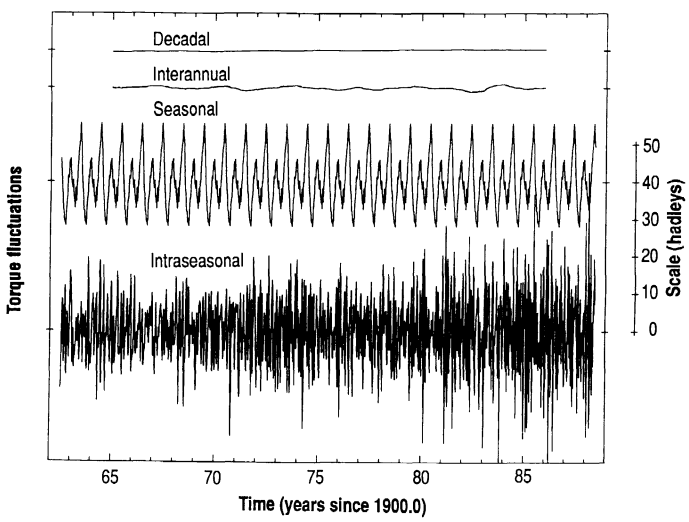

Fig. 4. Time series of the equivalent axial torques $\Gamma_\alpha(t)$, $\Gamma_\beta(t)$, $\Gamma_\gamma(t)$, and $\Gamma_\delta(t)$ from 1963 through 1988 corresponding respectively to the decadal $[\Lambda_\alpha(t)]$, interannual $[\Lambda_\beta(t)]$, seasonal $[\Lambda_\gamma(t)]$, and intraseasonal $[\Lambda_\delta(t)]$ spectral components $\Lambda^*(t)$ given in Fig. 2 (see Eqs. 5 and 6). Zero values are indicated on the left- and right-hand borders of the figure.

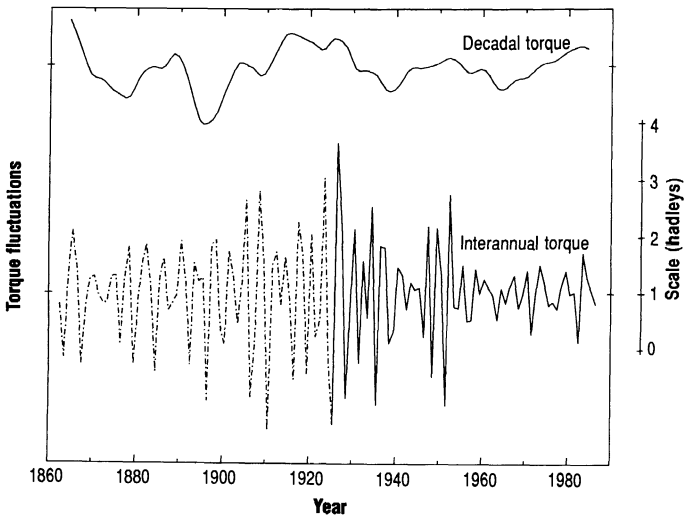

Fig. 5. Time series of the equivalent axial torques $\Gamma_\alpha(t)$ and $\Gamma_\beta(t)$ from 1860 through 1988 corresponding respectively to the decadal $[\Lambda_\alpha(t)]$ and interannual $[\Lambda_\beta(t)]$ spectral components of the time series $\Lambda^*(t)$ presented in Fig. 3. Effects of random errors in $\Lambda_\beta(t)$ dominate the $\Gamma_\beta(t)$ time series before 1925 (see text). Zero values are indicated on the left- and right-hand borders of the figure.

time rate of change of the total angular momentum of the core [but see (*13*)]. So discussions of the interpretation of $\Lambda_\alpha(t)$ have usually been concerned with the nature of the torques themselves, which must be adequate both quantitatively and qualitatively to account for the $\Gamma_\alpha(t)$ time series (Fig. 5).

The hydrodynamical stresses at the CMB comprise (i) tangential stresses produced by viscous forces in the thin Ekman-Hartmann boundary layer just below the core-mantle interface and also by Lorentz forces associated with the interaction of electric currents in the weakly conducting lower mantle with the magnetic field there and (ii) normal stresses produced largely by dynamical pressure forces acting on interface topography (that is, departures in shape from that of a sphere) (*25*). Insufficient knowledge of core motions, the viscosity and electrical conductivity of the core and the electrical conductivity of the lower mantle and the magnetic field there, and the topography of the core-mantle interface make it impossible to determine the torque acting at the CMB with much certainty. But progress is now accelerating as geophysicists intensify their studies of the structure, composition, and dynamics of the Earth's deep interior (*12, 13*).

Although not completely certain, viscous coupling is likely negligible, so most investigations are concerned with electromagnetic coupling or topographic coupling. The strength of electromagnetic coupling depends critically on the assumed electrical conductivity of the lower mantle and the assumed intensity of the magnetic field (poloidal and toroidal) at the core-mantle interface, and it would be zero in the case of a perfectly insulating mantle. The strength of topographic coupling depends on the assumed amplitude of the topography, but not in a monotonic way owing to subtle effects related to the intensity and structure of the magnetic field at the core-mantle interface and elsewhere within the core and also to horizontal density variations that are proportionately tiny but dynamically significant (*2, 4, 12, 13, 25*).

An essential step in the estimation of both the electromagnetic and topographic torques from geophysical observations is the determination of the geomagnetic field and its time rate of change at the CMB. This is done by downward extrapolation of the main geomagnetic field and its secular changes as measured at and near the Earth's surface, a procedure that places great demands on attempts to improve geomagnetic observations and methods of error analysis. From determinations of the geomagnetic field near the CMB it is possible under plausible assumptions to determine the horizontal velocity and pressure fields in the outer core. These pressure fields can be combined with various models of the topography of the core-mantle interface (based on gravity data, seismic tomography, and various assumptions about the rheology of the mantle and the structure of the so-called D'' layer at the base of the mantle) to produce hypothetical values of the topographic torque at the core-mantle interface (*10, 12, 13, 26*). One can find hypothetical values of the electromagnetic torque by calculating the Lorentz forces in the lower mantle under various assumptions concerning the electrical conductivity and magnetic field fluctuations there (*30, 31*).

Acceptable models of the Earth's deep interior must be such that the total hypothetical torque (topographic plus electromagnetic) agrees satisfactorily with the $\Gamma_\alpha(t)$ time series [and the corresponding equatorial component of the torque must agree with determinations of polar motions on decadal time scales (*12, 26*)]. Of particular interest are the extreme cases when one or the other type of coupling dominates, even though further studies might show that both are comparable in importance. The study of core-mantle coupling in connection with the interpretation of decadal variations in the Earth's rotation bears directly on the problem of accounting for the main geomagnetic field in terms of self-exciting magnetohydrodynamic dynamo action in the core.

Dynamo models can be classified in terms of two characteristic features. The first is the ratio of the strengths of the toroidal and poloidal magnetic fields in the core, which in strong field dynamos is much greater than unity and in weak field dynamos is of the order of unity. The second is the extent to which dynamo action is concentrated in the upper reaches of the core or extends throughout the whole body of the core. Topographic coupling might account for the observed decadal changes in the Earth's rotation if Lorentz forces associated with strong toroidal magnetic fields are restricted to the deep interior of the core. More extensive and refined calculations that either weaken the case for significant topographic coupling or consistently indicate excessive topographic coupling would constitute evidence in favor of strong electromagnetic torques at the CMB, produced by dynamo action concentrated just below the CMB.

On the basis of the hypothesis that electromagnetic and viscous coupling are negligible in comparison with topographic coupling, the torque **L** applied by the core to the solid Earth is given by

$$\mathbf{L}(t) = c^2 \int_0^{2\pi} \int_0^{\pi} (\mathbf{r} \times h \nabla_s p_s) \sin\theta d\theta d\lambda \qquad (7)$$

[see Eqs. 2.5 to 2.9 in (*12*)], where θ denotes co-latitude, λ longitude, and the (nearly spherical) shape of the CMB is the locus of points where the distance from the Earth's center of mass is equal to $c + h(\theta, \lambda)$, c being the mean radius of the CMB (3480 k) and the poorly known topography h (θ, λ) is such that $|h| \ll c$. The quantity p_s is the dynamic pressure associated with core motions $\mathbf{u}_s$ in the free stream just below the viscous boundary layer at the CMB and the operator

$$\nabla_s \equiv c^{-1}(\hat{\boldsymbol{\theta}}\partial/\partial\theta, \hat{\boldsymbol{\lambda}}\mathrm{cosec}\theta\partial/\partial\lambda) \qquad (8)$$

if $\hat{\boldsymbol{\theta}}$ and $\hat{\boldsymbol{\lambda}}$ are unit vectors in the directions of increasing θ and λ, respectively. If we assume that there is geostrophic balance at that level, the term $\nabla_s p_s$ can be replaced by $-2\bar{\rho}\,\boldsymbol{\Omega} \times \mathbf{u}_s$ (where $\bar{\rho}$ is the horizontally averaged value of the density in the upper reaches of the core), giving for the axial component of $\mathbf{L}(t)$ the expression

$$-2\Omega_0\bar{\rho}\int_0^{2\pi}\int_0^{\pi} h(\theta,\lambda)\nu_s \sin^2\theta \cos\theta \, d\theta \, d\lambda \qquad (9)$$

where v_s is the θ component of $\mathbf{u}_s$. The axial component of $\mathbf{L}$ (unlike the equatorial components) depends on λ-dependent features of h. These features are not known with any degree of confidence, in spite of efforts made over several decades to infer h (θ, λ) from the pattern of long-wave anomalies of the Earth's gravitational field under various assumptions about the structure and rheology of the solid Earth or, as in more recent studies, from the results of seismic tomography. The quantity $\mathbf{u}_s(t)$ is obtained from determinations of the geomagnetic secular variation at the CMB using "Alfvén's frozen magnetic flux" hypothesis and the geostrophic relationship (*10, 12, 13, 27*).

Rough dynamical arguments (*2, 25*) show that even with a high degree of canceling of positively and negatively directed contributions to the axial component of $\mathbf{L}$ the presence of λ-dependent variations in h of no more than 0.5 km in effective amplitude should suffice to account for the magnitude of $\Gamma_\alpha(t)$ inferred through Eq. 9; more detailed calculations based on Eq. 9 confirm this result (*27*). Moreover, these findings are consistent with an estimate of 0.5 km for the excess ellipticity of the CMB inferred from determinations of the amplitude and phase of the "free-core nutation" (*32–36*) and also from models of irregular CMB topography based on seismic data that allow for mechanical and chemical variations in the D'' layer at the base of the mantle (*26*).

The foregoing arguments have to be modified slightly if between the fluid metallic core and the overlying mantle there exist either a continuous layer or pools of poorly conducting fluid (*12, 27*). The effective topography in Eqs. 7 and 9 could then be significantly less than the actual topography of the CMB, a situation that might appeal to those seismologists who advocate models of irregular CMB topography with amplitudes of several kilometers (*12, 13, 27*).

Interannual, Seasonal, and Intraseasonal Fluctuations

Fluctuations in the rotation of the solid Earth over time scales of less than about 2 years are dominated by atmospheric effects. Many detailed studies of these fluctuations and compensating fluctuations in the angular momentum of the atmosphere have been reported in the past decade. Research in this area has been facilitated by the use of the dimensionless atmospheric angular momentum (AAM) functions $\chi_i (i = 1, 2, 3)$ (Fig. 1). In this scheme the excitation of polar motion is determined by $\chi_1(t)$ and $\chi_2(t)$ and that of axial rotation variation by $\chi_3(t)$. It is the χ_i functions that are issued routinely by meteorological agencies. The axial component χ_3 is given by

$$\chi_3 \equiv \frac{0.70R^4}{gC}\int_{-\pi/2}^{\pi/2}\int_0^{2\pi} p_s \cos^3\phi \, d\lambda \, d\phi + \frac{R^3}{gC\Omega_0}\int_0^{p_s}\int_{-\pi/2}^{\pi/2}\int_0^{2\pi} u \cos^2\phi \, d\lambda \, d\phi \, dp \qquad (10)$$

where ϕ and λ denote latitude and longitude respectively, p_s (ϕ, λ, t) is the surface pressure, $u(\phi, \lambda, p, t)$ represents the eastward (westerly) component of the wind velocity at the pressure level p, R is the mean radius of the Earth (6.37×10^6 m), and $g = 9.81$ m s^{-2} is the mean acceleration due to gravity (*16*). The coefficient 0.70 incorporates the "Love-number" correction, which allows for concomitant changes in the inertia tensor of the imperfectly rigid solid Earth. Small effects arising from the contribution of water vapor to the surface pressure distribution are not allowed for in this approximation.

Routine daily or twice daily determinations of χ_i are now produced at four meteorological forecasting centers: the European Centre for Medium-range Weather Forecasts (EC), the Japanese Meteorological Agency, the U.K. Meteorological Office, and the U.S. National Meteorological Center (NMC). Several atmospheric variables, including the surface pressure and the vertical distribution of the horizontal components of the local wind velocity vector, are estimated at each model grid point. The grid point data are updated several times daily by means of a forecast assimilation scheme, in which weighted means of data from the earlier forecast and any new observational material are used (*37*). Changes in the angular momentum of the atmosphere are thus estimated at 12- or 24-hour intervals (depending on the service used) from the appropriate volume integral over the whole atmosphere.

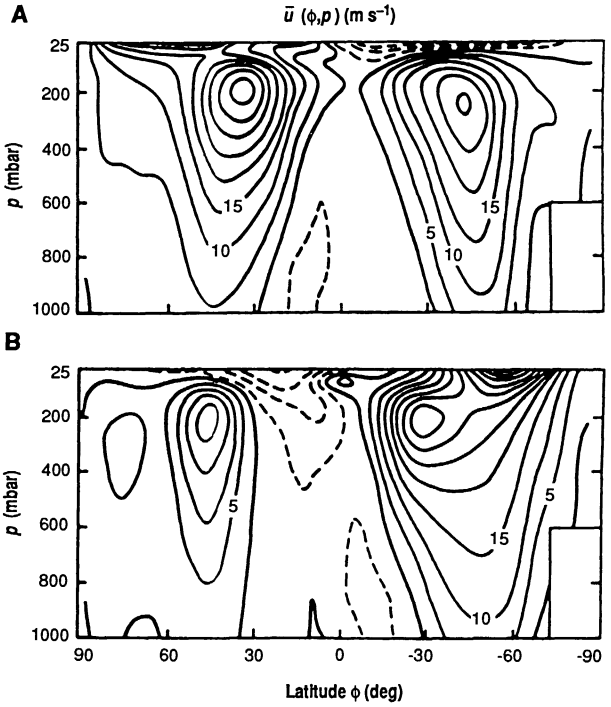

Fig. 6. The pressure level–latitude distribution within the atmosphere of $\bar{u}$ (ϕ, p) (m s^{-1}), the monthly mean value of the zonal average of the eastward (westerly) component u (ϕ, λ, p, t) of the wind for (**A**) January 1988 and (**B**) July 1988 [see (*97*), Fig. 2]. The data are based on EC analyses of routine meteorological observations.

The AAM changes can be divided into two categories: changes in the net atmospheric rotation rate (the wind term represented by second integral in Eq. 10) and changes in the net atmospheric moment of inertia (the pressure term represented by the first integral). The dominant contribution to fluctuations in χ_3 [and to the compensating fluctuations in $\Lambda_\beta(t)$, $\Lambda_\gamma(t)$, and $\Lambda_\delta(t)$] originates from the wind term; the pressure term generally contributes no more than about 10%. A rough allowance for the response of the oceans to atmospheric surface pressure changes can be made by the inverted barometer correction, which assumes that the oceans are able to reach equilibrium with the surface loading (*16*). The average eastward wind velocity distribution is shown in Fig. 6 as a function of pressure and latitude. The maximum velocities are found in the upper level jet streams in the subtropics, which contribute a substantial fraction of the global AAM variability (*38*).

Conservation of angular momentum implies that any change $\Delta\chi_3$ in χ_3 is accompanied by a change in Λ^* equal to $-\Lambda_0\Delta\chi_3$ [because fluctuations in the azimuthal motion of the liquid core are effectively decoupled from those of the solid Earth on these short time scales (*39*)]. If we define a quantity $X(t)$ with the dimension of seconds as follows:

$$X(t) \equiv \Lambda_0\chi_3(t) \qquad (11)$$

then $\Lambda(t)$ and $\chi(t)$ satisfy

$$\dot{\Lambda}(t) = \dot{X}(t) + \text{terms due to nonmeteorological excitation} \quad (12)$$

We further define $X^I(t)$ to be the estimate of $X(t)$ obtained from the service denoted by the superscript I [for example, $X^{NMC}(t)$ for data from the NMC].

Historically, comparison of astronomical measurements with axial atmospheric angular momentum first indicated the significance of the atmospheric contribution to Earth's rotation. Various studies [such as (*40–42*)] have related fluctuations in Λ_β, Λ_γ, and Λ_δ to changes in atmospheric angular momentum on time scales ranging from months to a few years, on the basis of mean monthly or longer period atmospheric data. The analysis of the zonal component of angular momentum at 12-hour intervals from the First GARP (Global Atmosphere Research Program) Global Experiment (FGGE) along with concurrent LOD data obtained by classical optical techniques demonstrated good agreement between these two data types and indicated that angular momentum transfer between the Earth and atmosphere could fully account for the observed rotational variation on the time scale of days to weeks (*39*). Intercomparisons of AAM data with modern LOD data obtained from space geodetic techniques (see for example, Fig. 7) have been at the forefront of recent research on seasonal and subseasonal fluctuations in the Earth's angular momentum budget (*38, 43–47*). These studies indicate that the difference between any two AAM time series is comparable to their difference with LOD, implying that the noise levels in the two data types are comparable (*46, 48*).

Various studies of the small apparent discrepancies found in these intercomparisons (*45, 47*) reveal that imbalances occur in the angular momentum budget at the semiannual period and to a lesser extent at the annual period. Most of the semiannual imbalance can be attributed to the failure to represent the contribution from stratospheric winds satisfactorily in some routine operational analyses (*49*), but changes in the oceanic circulation may have to be invoked to account for small seasonal imbalances that occur (*45, 50, 51*). A recent study (*52*) of likely contributions from the movement of ground water and fluctuations in the Antarctic circumpolar current to the Earth's angular momentum budget at seasonal periods

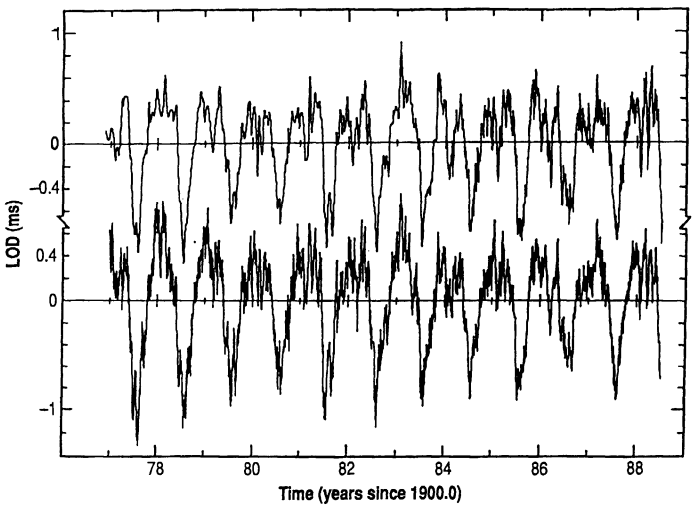

Fig. 7. Time series of the sum of the seasonal and intraseasonal components $[\Lambda_\gamma(t) + \Lambda_\delta(t)$ of $\Lambda^*(t)$, see Eq. 4] (upper curve, measured by space geodetic techniques) and the contribution $X^{NMC}(t) \equiv \Lambda_0\chi_3{}^{NMC}(t)$ (see Eq. 11) to $\Lambda_\gamma(t) + \Lambda_\delta(t)$ expected from atmospheric excitation (lower curve), as determined from routine daily determinations of changes in the axial component of the angular momentum of the atmosphere made by the U.S. National Meteorological Center (see text).

was able to reduce small discrepancies at the annual period, but an apparent discrepancy of about 6%, possibly associated with errors in the data, is still present at the semiannual period.

Superimposed on the annual cycle in both types of data is the irregular "intraseasonal" fluctuation, evident on time scales ranging from roughly 30 to 60 days. This oscillation is associated with fluctuations in zonal winds and other meteorological quantities on these time scales, which were first noticed in data from the equatorial Pacific (*53, 54*). Since that time, intraseasonal oscillations with higher frequency have also been seen (*55–57*), and the 30- to 60-day oscillation has been observed on a global scale (*58–60*). Corresponding Earth rotation changes were first detected in optical data (*61*) and later confirmed by their presence in four independent LOD data types (*62*). These were related to the AAM oscillation through the analysis of LLR data (*43*). The peak amplitude is about 0.2 ms in LOD, although the oscillation exhibits changes in both period and amplitude on a year-to-year basis (*63, 64*). Any nonmeteorological contribution to the 30- to 60-day oscillation is not significantly larger than the uncertainties in the observations (about 0.06 ms) (*47*).

Several mechanisms for the 30- to 60-day oscillation have been proposed. One theory, denoted here as the "Madden-Julian" (MJ) mechanism, connects these intraseasonal LOD and AAM variations to anomalies in tropical convection and zonal wind (*53, 54*). The observed near-periodicity is assumed to result from the transit time of these convectively driven waves around the equator (*65, 66*) or from a combination of such tropical waves and of extratropical Rossby waves traveling along an approximate great circle route involving legs in the Northern (*67*) or Southern (*68*) Hemisphere extratropics.

A second hypothesis (*69, 70*) relates the oscillation to an instability of nonzonal westerly flow caused by the interaction of jet streams with mountain ranges in the mid-latitudes. The dominant period of this instability in a simplified, equivalent-barotropic model of the atmosphere (*71*) is close to 40 days, but for realistic parameter values the model exhibits aperiodic behavior, which might account for the broadband nature of the oscillations in AAM and hence Λ_δ. Barotropically unstable modes with periods near 50 days have been found in the climatological mean winter circulation of the Northern Hemisphere at 300 mbar (*72*); another proposed mechanism relates low-frequency variability of the wintertime general circulation of the Northern Hemisphere to disturbances that derive their energy from the basic state through barotropic instability. In this third theory, topography contributes only to the maintenance of asymmetries in the climatological basic state and plays no direct role in the instability mechanism itself. In the second approach, topography interacts both with the basic flow and with its oscillatory instability.

The analysis of Earth rotation variations in concert with AAM data provides insights into the intraseasonal oscillation and other geophysical processes. Studies of the spectral characteristics of signal-to-noise ratios in both data types, for example, indicate that Λ_δ determinations give a more accurate picture of 30- to 60-day variations in the global angular momentum budget than can be obtained at present from the available AAM determinations (*73*). By compositing Earth rotation data over several years, the global intraseasonal oscillation was found to be strongest during Northern Hemisphere winter (*64*). These data indicate that the low-frequency variability of the Northern Hemisphere extratropics may be important to the dynamics of the global oscillation, as envisaged in the second and third hypotheses (*64, 74*).

Spectral analysis of modern LOD data shows the presence of two distinct intraseasonal oscillations having periods near 50 and 40 days, respectively. Studies of concurrent AAM variations from the NMC operational analysis and perpetual-January runs with the

UCLA General Circulation Model indicate that the larger amplitude 50-day oscillation arises in the tropics, whereas the 40-day oscillation originates in the Northern Hemisphere extratropics. Thus, comparisons of geodetically determined Λ_δ values with both observed and simulated AAM data indicate that the global intraseasonal oscillation may result from a combination of all three aforementioned mechanisms (*64, 74*).

The largest deviations (0.7 ms) from the annual running mean value of both AAM and Λ (Λ_δ, see Fig. 2) over the 12-year span of overlapping data occurred in early 1983 (Fig. 7). Unusually large changes in Λ_δ and global AAM took place during January and February of that year (Fig. 8). These anomalies coincided with the most intense period of the 1982 to 1983 El Niño and unusual changes in the atmospheric pressure distribution over the eastern and western tropical Pacific Ocean. Earth rotation measurements from the four observing networks permitted this Λ_δ event to be monitored in detail. The 1983 burst is approximately four standard deviations from the seasonal mean value for both the Kalman-smoothed $\Lambda(t)$ series and the two AAM time series then available, from the NMC and the EC. These were the largest such deviations ever reported for either Λ or the global AAM (*75*). Comparison of the variations in AAM and LOD indicates that the Earth responds to atmospheric torques at high frequencies with no discernible lag or lead.

The elucidation of the relation between Λ and X at high frequencies is important in investigations of the Earth's angular momentum budget (*73, 76*). A recent study found that significant coherence between modern estimates of these two data types is lost at periods shorter than about 2 weeks (*76*). By using stochastic models of the geophysical processes and measurement errors involved to calculate the expected coherence as a function of frequency, researchers have extended the limit of significant coherence down to about 10 days (*73*). The loss of coherence at 2 weeks is probably due to limitations in the tidal model used for Λ_2 excitations; discrepancies in the signal occur at the same level as the quoted uncertainties in the tidal model. At periods shorter than 10 days, the lack of coherence can be attributed to low signal-to-noise ratios, which decrease with increasing frequency in both Λ and X data sets. Thus there is no need at present to invoke significant nonmeteorological excitation in the interpretation of Λ_δ (*73*); however, more frequent and accurate determinations of both X and Λ are required in order to balance the Earth's angular momentum budget at high frequencies.

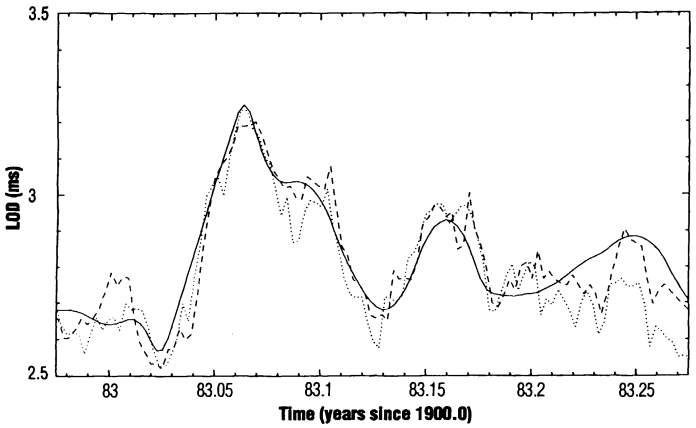

Fig. 8. Comparison between Λ^* determined from the combined Kalman-smoothed LOD estimates and X^{EC} and X^{NMC} (solid line, smoothed LOD; dashed line, NMC AAM; dotted line, EC AAM) inferred from routine atmospheric angular momentum determinations made by the EC and the NMC during the northern winter of 1982–83 (the occasion of one of the most intense ENSO events on record).

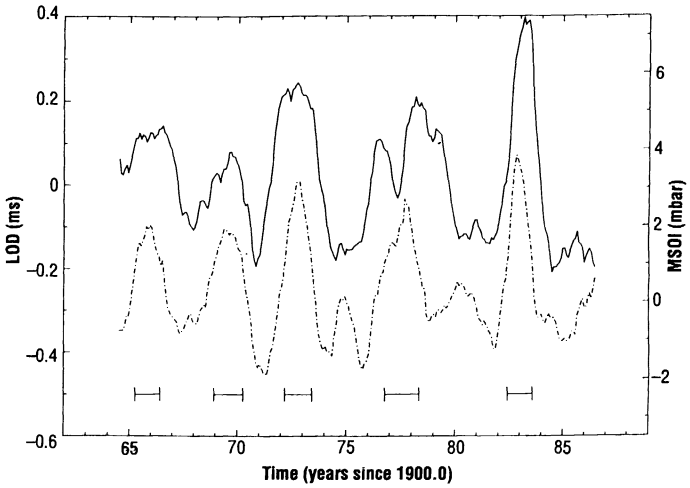

Fig. 9. The interannual LOD variation (upper curve) Λ_β and the MSOI (lower curve) from 1964 through 1986. The MSOI is defined as the negative of the 1-year moving average of the Southern Oscillation Index. ENSO events are denoted by the bars at the bottom (*19*).

Changes in $\Lambda^*(t)$ at seasonal and higher frequencies [$\Lambda_\gamma(t)$ and $\Lambda_\delta(t)$], therefore, can be attributed primarily to exchange of angular momentum with the atmosphere, with zonal frictional stress and surface pressure gradients acting as agents for transferring angular momentum between the atmosphere and the Earth. At the other end of the frequency domain, tidal dissipation, postglacial rebound, and core-mantle interactions are accepted as the causes of the long-term (secular to decade) variations in $\Lambda_\alpha(t)$. Between these regimes fall the interannual variations $\Lambda_\beta(t)$, which encompass fluctuations with periods from 1 to 5 years. The similarity of the amplitude of these variations (~0.5 ms) to that of the seasonal cycle implies that the atmosphere could play a major role in their generation.

Several previous studies have linked the interannual $\Lambda_\beta(t)$ fluctuations to the stratospheric quasi-biennial oscillation (QBO), characterized by the regular alternation of the zonal wind in the equatorial stratosphere at a period that varies form 24 to 30 months [for a review, see (*3*)]. A connection between the $\Lambda_\beta(t)$ fluctuations and the Southern Oscillation was subsequently proposed on the basis of the observed high coherence between interannual fluctuations in Λ and equatorial Pacific air temperature (*77*). Further investigations were stimulated by the unusually strong and well-observed El Niño of 1982 to 1983, which was accompanied by the largest changes ever recorded in Λ and X (Figs. 7 and 8). The coupled El Niño–Southern Oscillation (ENSO) phenomenon involves a large-scale redistribution of atmospheric mass between the eastern and western ends of the Pacific basin and is associated with widespread changes in both atmospheric and oceanic circulation (*78*). Various studies (*19, 79–81*) have established significant correlations between $\Lambda_\beta(t)$ and the Southern Oscillation Index (SOI), computed as the seasonally adjusted difference of the sea level pressure between Tahiti and Darwin, Australia. A recent study (*82*) demonstrated that independent measures of the QBO and ENSO cycles, when analyzed jointly, yield improved correlations with $\Lambda_\beta(t)$.

During an ENSO event the SOI reaches a minimum, and there is a concomitant collapse of the tropical easterlies and an increase in χ_3. Conservation of total angular momentum requires the Earth's rate of rotation to diminish, causing Λ to increase. A further increase in AAM may result from the large-scale heating of the tropical troposphere associated with the El Niño events (*77*), leading to a zonally symmetric rise in the tropical 200-mbar height field (*83*) and a consequent strengthening of the upper level subtropical jet

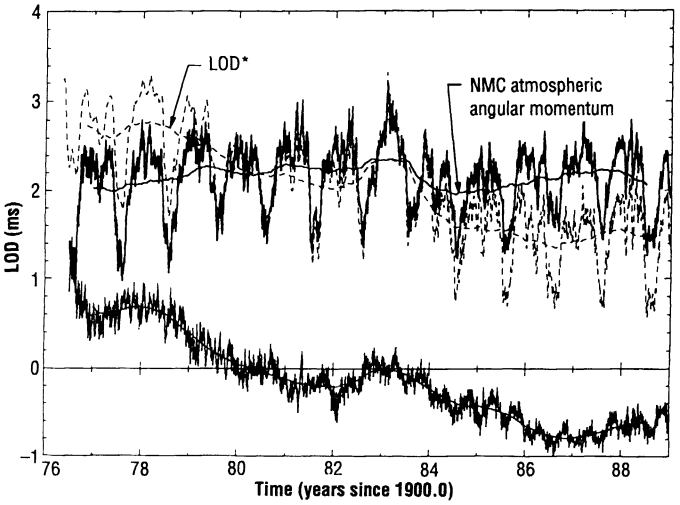

Fig. 10. Determinations of residual length-of-day variations from 1976 to 1986 after tidal variations have been removed. Two data sets are displayed: (i) the Kalman-smoothed length-of-day time series (Λ^*) and (ii) X^{NMC} as inferred from atmospheric angular momentum calculated by the NMC. The lower curve is the difference between these two series. Associated with each series are the results of eliminating the shortest period contributions and the seasonal effects by taking a 365-day running mean, leaving interannual and decade contributions. Note the enhancements in the difference curve during the El Niño periods (1977–78 and 1982–83). [adapted from (*19*)]

streams. Almost all of the anomalous AAM variations associated with the 1982 to 1983 event, the largest on record, were found to occur in the Northern Hemisphere subtropics (*19, 84*).

The striking agreement between the interannual LOD variation (Λ_β) and the MSOI (a modified Southern Oscillation index, formed by taking the negative of the running annual SOI variation) is evident in Fig. 9 (after *19*). Similar comparisons have been made with data sets beginning in the 1880s (*19, 85*). Results indicate correlations robust enough that $\Lambda_\beta(t)$ can be used as a proxy index of interannual global wind fluctuations beginning in about 1925. The maximum cross correlation in the modern data (0.72) is found with the MSOI leading variations in Λ_β (and in the transfer of angular momentum to the solid Earth) by about 2 months. This time lag is consistent with the growth and development of an El Niño event and, in particular, the onset of ENSO's teleconnection with pressure fields in Northern Hemisphere extratropical latitudes (*80, 83*). The mountain torque, because of horizontal pressure gradients acting over zonally varying topography, occurs mainly in the Northern Hemisphere extratropics. It is a major agent for transferring angular momentum between the atmosphere and the solid Earth on short time scales (*86–89*) and may be the dominant physical mechanism that connects the ENSO phenomenon with Λ_β variations (*84, 87*).

Much can be learned through the comparison of concurrent AAM (X^i_3) and Λ time series and the examination of their residual, which indicates systematic errors, omission in the atmospheric data, or additional sources of excitation (Fig. 10). The X^{NMC} time series that we have used, for example, incorporates data up to 50 mbar; hence, the very highest part of the atmosphere is not included. The difference between the X^{NMC} and the Λ time series (*19, 76*) (Fig. 10) shows a seasonal error caused in large part by the neglect of the upper atmosphere in routine AAM calculations (*48*), significant interannual variations in slope with enhancements during the El Niño periods (1977–78 and 1982–83), and the long-term linear drift associated with the decade variations.

We have further investigated the interannual component of the Λ-AAM discrepancy using an atmospheric data set extending to the 1 mbar level for the 1980 to 1986 period, which included the usually strong 1982–83 El Niño (*19*). Atmospheric winds were found to be the dominant cause of the Λ_β variations; the X^{NMC} series integrated up to 100 mbar accounted for 66% of the interannual variance, and a series incorporating winds up to 1 mbar accounted for 89% of the variance. This comparison suggests that the stratosphere is important to the Earth's angular momentum budget on interannual time scales. The remaining 11% of the Λ_β variance, with root mean square amplitude of 0.04 ms, cannot be accounted for with the available atmospheric data sets; thus, exchange with another reservoir of angular momentum may play a significant role on these time scales, or there may be systematic problems with the current atmospheric models or data sets or both.

In this context, the size of the remaining interannual discrepancy between modern geodetic and atmospheric data is now at the level where the oceanic effects may be detectable. An oceanic current with a transport of 40 Sv between the western and eastern equatorial Pacific, for example, could account for the 0.04-ms residual in Λ_β, and several observational studies [such as (*90*)] and model simulations [such as (*91, 92*)] have detected anomalous current systems of the required magnitude associated with ENSO events. As geodetic, atmospheric, and oceanic observational techniques continue to improve, it appears likely that the remaining discrepancies in the Earth's angular momentum budget can be quantitatively resolved for variations on intraseasonal to interannual time scales.

REFERENCES AND NOTES

1. W. H. Munk and G. J. F. Macdonald, *The Rotation of the Earth* (Cambridge Univ. Press, London, 1960).
2. R. Hide, *Philos. Trans. R. Soc. London Ser. A* **284**, 547 (1977).
3. K. Lambeck, *The Earth's Variable Rotation* (Cambridge Univ. Press, London, 1980).
4. M. G. Rochester, *Philos. Trans. R. Soc. London Ser. A* **313**, 95 (1984).
5. R. Hide, *ibid.*, p. 107.
6. A. Cazenave, Ed., *Earth Rotation: Solved and Unsolved Problems*, vol. 187 of *NATO Adv. Inst. Ser. C* (Reidel, Dordrecht, Holland, 1986).
7. J. O. Dickey and T. M. Eubanks, in *Space Geodesy and Geodynamics*, A. J. Anderson and A. Cazenave, Eds. (Academic Press, New York, 1986), pp. 221–267.
8. J. M. Wahr, in *Space Geodesy and Geodynamics*, A. J. Anderson and A. Cazenave, Eds. (Academic Press, New York, 1986), pp. 281–314.
9. H. Moritz and I. I. Mueller, *Earth Rotation: Theory and Observation* (Ungar, New York, 1987).
10. D. Jault, C. Gire, J-L. Le Mouël, *Nature* **333**, 353 (1988).
11. J. M. Wahr, *Annu. Rev. Earth Planet. Sci.* **16**, 231 (1988).
12. R. Hide, *Philos. Trans. R. Soc. London Ser. A* **328**, 351 (1989).
13. D. Jault and J. L. Mouël, *Geophys. J. Int.* **101**, 233 (1990).
14. J. M. Wahr, *Geophys. J. R. Astron. Soc.* **70**, 349 (1982).
15. ———, *ibid.* **74**, 451 (1983).
16. R. T. H. Barnes *et al.*, *Proc. R. Soc. London* **387**, 31 (1983).
17. T. M. Eubanks *et al.*, *Nature* **334**, 115 (1988).
18. C. F. Yoder, M. W. Parke, J. G. Williams, *J. Geophys. Res.* **86**, 881 (1981).
19. J. O. Dickey, T. M. Eubanks, R. Hide, *Geophys. Monogr. Am. Geophys. Union* **59**, 157 (1990); J. O. Dickey, S. L. Marcus, R. Hide, T. M. Eubanks, in preparation.
20. R. D. Rosen, D. A. Salstein, T. M. Wood, *J. Geophys. Res.* **96**, 5145 (1991).
21. T. M. Eubanks, in *BIH Annual Report for 1987*, M. Feissel, Ed. (Observatoire de Paris, Paris, 1988), p. D85.
22. D. D. Morabito, T. M. Eubanks, J. A. Steppe, in *The Earth's Rotation and Reference Frames for Geodesy and Geodynamics*, A. K. Babcock and G. A. Wilkins, Eds. (Kluwer Academic, Dordrecht, Holland, 1988), pp. 257–268.
23. A. P. Anufriev and S. I. Braginsky, *Geomagn. Aeron. (U.S.S.R.)* **17**, 78 (1977); *ibid.*, p. 492.
24. I. A. Eltayeb and M. H. A. Hassan, *Physics Earth Planet. Inter.* **19**, 239 (1979).
25. R. Hide, *Nature* **222**, 1055 (1969).
26. ———, *Q. J. R. Astron. Soc.* **278**, 3 (1986).
27. ———, *Surv. Geophys.* **11**, 340 (1990); ———, R. W. Clayton, B. H. Hager, M. A. Spieth, C. V. Voorhies, in preparation.
28. J. A. Jacobs, Ed., *Geomagnetism* (two volumes) (Academic Press, New York, 1987).
29. H. K. Moffatt, *Magnetic Field Generation by Fluid Motion* (Cambridge Univ. Press, London, 1978).
30. M. Paulus and M. Stix, *Geophys. Astrophys. Fluid Dyn.* **47**, 237 (1989).
31. P. H. Roberts, *ibid.* **44**, 181 (1988).
32. T. M. Eubanks, J. A. Steppe, O. J. Sovers, in *Proceedings of the International Conference on Earth Rotation and Terrestrial Reference Frame*, Ohio State University, 31 July to 2 August 1985, I. I. Mueller, Ed. (Ohio State University, Columbus, OH, 1985), pp. 326–340.
33. T. A. Herring, C. R. Gwinn, I. I. Shapiro, in *ibid.*, pp. 307–325.
34. ———, *J. Geophys. Res.* **91**, 4745 (1986).

35. C. R. Gwinn, T. A. Herring, I. I. Shapiro, *ibid.*, p. 4755.
36. J. Neuberg, J. Hinderer, W. Zurn, *Geophys. J. R. Astron. Soc.* **91**, 853 (1987).
37. R. D. McPherson *et al.*, *Mon. Weather Rev.* **107**, 1445 (1979).
38. R. D. Rosen and D. A. Salstein, *J. Geophys. Res.* **88**, 5451 (1983).
39. R. Hide *et al.*, *Nature* **286**, 114 (1980).
40. W. Rudloff, *Ann. Meteorol. Neue Folge* **6**, 221 (1973).
41. K. Lambeck and A. Cazenave, *Philos. Trans. R. Soc. London Ser. A* **284**, 495 (1977).
42. K. Lambeck and P. Hopgood, *Geophys. J. R. Astron. Soc.* **71**, 581 (1982).
43. R. B. Langley *et al.*, *Nature* **294**, 730 (1981).
44. W. E. Carter *et al.*, *Science* **224**, 957 (1984).
45. T. M. Eubanks *et al.*, *J. Geophys. Res.* **90**, 5385 (1985).
46. J. O. Dickey, T. M. Eubanks, J. A. Steppe, in (*6*), pp. 137–162.
47. P. J. Morgan, R. W. King, I. I. Shapiro, *J. Geophys. Res.* **90**, 12645 (1985).
48. R. D. Rosen *et al.*, *Mon. Weather Rev.* **115**, 1627 (1987).
49. R. D. Rosen and D. A. Salstein, *J. Geophys. Res.* **90**, 8033 (1985).
50. P. Brosche and J. Sündermann, *Dtsch. Hydrogr. Z.* **38**, 1584 (1985).
51. C. M. Johns, J. O. Dickey, T. M. Eubanks, J. A. Steppe, *Eos* **68**, 1244 (1987).
52. I. Naito and N. Kikuchi, *Geophys. Res. Lett.* **17**, 5 (1990).
53. R. A. Madden, *J. Geophys. Res.* **92**, 8391 (1987).
54. ———, *ibid.* **93**, 5333 (1988).
55. A. J. Miller, *J. Atmos. Sci.* **31**, 720 (1974).
56. G. Branstator, *ibid.* **44**, 2310 (1987).
57. M. Ghil and K. Mo, *ibid.* **48**, 752 (1991).
58. J. D. Anderson and R. D. Rosen, *ibid.* **40**, 1584 (1983).
59. T. M. Krishnamurti and D. Subrahmanyam, *ibid.* **39**, 2088 (1982).
60. T. Yasunari, *J. Meteorol. Soc. Jpn.* **59**, 336 (1981).
61. Zheng Da-Wei, *Chin. Astron. Astrophys.* **3**, 114 (1979).
62. M. Feissel and D. Gambis, *C. R. Acad. Sci. Ser. II* **291**, 271 (1980).
63. M. Feissel and C. Nitschelm, *Ann. Geophys.* **3**, 180 (1985).
64. J. O. Dickey, M. Ghil, S. L. Marcus, *J. Geophys. Res.*, in press; in *The Earth's Rotation and Reference Frames for Geodesy and Geodynamics*, C. Boucher and G. A. Wilkins, Eds. (Springer-Verlag, New York, 1990), pp. 90–97.
65. A. C. Lorenc, *Q. J. R. Meteorol. Soc.* **110**, 427 (1984).
66. K. M. Lau and L. Peng, *J. Atmos. Sci.* **44**, 950 (1987).
67. K.-M. Lau and T. J. Phillips, *ibid.* **43**, 1164 (1986).
68. X. H. Gao and J. L. Stanford, *ibid.* **45**, 1425 (1988).
69. M. Ghil, in *Irreversible Phenomena and Dynamical Systems Analysis in Geosciences*, C. Nicolis and G. Nicolis, Eds. (Reidel, Dordrecht, Holland, 1987), p. 241.
70. ——— and S. Childress, *Topics in Geophysical Fluid Dynamics: Atmospheric Dynamics, Dynamo Theory and Climate Dynamics* (Springer-Verlag, New York/Berlin, 1987).
71. B. Legras and M. Ghil, *J. Atmos. Sci.* **42**, 433 (1985).
72. A. J. Simmons, J. M. Wallace, G. W. Branstator, *ibid.* **40**, 1363 (1983).
73. J. O. Dickey, S. L. Marcus, J. A. Steppe, R. Hide, *Eos* **70**, 1058 (1989).
74. S. L. Marcus *et al.*, in *The Earth's Rotation and Reference Frames for Geodesy and Geodynamics*, C. Boucher and G. A. Wilkins, Eds. (Springer-Verlag, New York 1990); S. L. Marcus, thesis, University of California, Los Angeles (1990).
75. T. M. Eubanks *et al.*, *Trop. Ocean Atmos. Newsl.* **29**, 21 (1985).
76. R. D. Rosen, D. A. Salstein, T. M. Wood, *J. Geophys. Res.* **95**, 265 (1990).
77. M. Stefanick, *ibid.* **87**, 428 (1982).
78. S. G. H. Philander, *El Niño, La Niña and the Southern Oscillation* (Academic Press, New York, 1990).
79. B. F. Chao, *Geophys. Res. Lett.* **11**, 541 (1984).
80. ———, *J. Geophys. Res.* **93**, 7709 (1988).
81. T. M. Eubanks, J. A. Steppe, J. O. Dickey, in (*6*), pp. 163–186.
82. B. F. Chao, *Science* **243**, 923 (1989).
83. J. D. Horel and J. M. Wallace, *Mon. Weather Rev.* **109**, 813 (1981).
84. R. D. Rosen *et al.*, *Science* **225**, 411 (1984).
85. D. A. Salstein and R. D. Rosen, *J. Clim. Appl. Meteorol.* **25**, 1870 (1986).
86. R. Swinbank, *Q. J. R. Meteorol. Soc.* **111**, 977 (1985).
87. W. L. Wolf and R. B. Smith, *J. Atmos. Sci.* **44**, 3656 (1987).
88. G. J. Boer, *J. Geophys. Res.* **95**, 5511 (1990).
89. J. M. Wahr, *J. Atmos. Sci.* **41**, 190 (1984).
90. K. Wyrtki, *J. Geophys. Res.* **89**, 10419 (1984).
91. Y. L. Jia, N. C. Wells, M. A. Rowe, *ibid.* **95**, 5395 (1990).
92. S. G. H. Philander and A. D. Seigel, in *Coupled Ocean-Atmosphere Models*, J. C. J. Nihoul, Ed. (Elsevier, New York, 1990), p. 517.
93. L. V. Morrison, *Geophys. J. R. Astron. Soc.* **58**, 349 (1979).
94. D. D. McCarthy and A. K. Babcock, *Phys. Earth Planet. Inter.* **44**, 281 (1986).
95. L. V. Morrison, *Mon. Not. R. Astron. Soc.* **187**, 41 (1979).
96. R. S. Gross, personal communication.
97. M. J. Bell *et al.*, *Philos. Trans. R. Soc. London Ser. A* **334**, 55 (1991).
98. The authors are grateful to D. L. Anderson, R. W. Clayton, T. M. Eubanks, A. P. Freedman, R. S. Gross, B. H. Hager, S. L. Marcus, R. D. Rosen, D. A. Salstein, M. A. Spieth, J. A. Steppe, C. V. Voorhies, and C. F. Yoder for useful discussions. Helpful comments on the manuscript were made by R. S. Gross and S. L. Marcus, who also assisted with the preparation of some of the diagrams. The work of one of the authors (J.O.D.) is the result of one phase of research carried out at the Jet Propulsion Laboratory, California Institute of Technology, sponsored by the National Aeronautics and Space Administration.

Molecular Recognition at Crystal Interfaces

I. WEISSBUCH, L. ADDADI, M. LAHAV, L. LEISEROWITZ

Nucleation, growth, and dissolution of crystals have been studied by stereochemical approach involving molecular recognition at interfaces. A methodology is described for using "tailor-made" additives designed to interact stereospecifically with crystal surfaces during growth and dissolution. This procedure was instrumental in controlling crystal morphology and in revising the concept of the structure and symmetry of solid solutions. Consequently, it was applied to the transformation of centrosymmetric single crystals into solid solutions with polar arrangement displaying second-harmonic generation and to the performance of asymmetric synthesis of guest molecules inside centrosymmetric host crystals. The method has led to a discovery of a new "relay" mechanism explaining the effect of solvent on crystal growth. Finally, it allowed for the design of auxiliary molecules that act as promoters or inhibitors of crystal nucleation that can be used to resolve enantiomers and crystallize desired polymorphs.

MOLECULAR RECOGNITION AT INTERFACES, SELF-ASSEMBLY, nucleation, and growth, are concepts of central importance in physics, chemistry, and biology. These concepts are manifest in crystals which, in their different functions and forms, are basic components of the world surrounding us, from minerals, ceramics, and microelectronic components, to bone, shells, and teeth.

Growing crystal surfaces can be thought of as being composed of "active sites" that interact stereospecifically with molecules in solution, in a manner similar to the interactions of enzymes and substrates or antibodies and antigens. At the same time, the highly ordered, repetitive arrangements at crystal surfaces, and the knowledge we have of their structures, offer simpler means to pinpoint

Department of Structural Chemistry, The Weizmann Institute of Science, Rehovot 76100, Israel.